UDC 551.2, 551.14, 550.423

Correlation of oxygen fugacity in the mantle lithosphere between Ce^{+4}/Ce^{+3} relation of zircons and petrological buffer FMQ

Balashov Yu.A.[1], Martynov E.V.[1,2]
[1] *Geological Institute, KSC RAS, Apatity*
[2] *Apatity Branch of MSTU, Geology and Minerals Department*

Abstract. The paper presents variations of Ce^{+4}/Ce^{+3} and Eu^{+3}/Eu^{+2} in zircons from different mantle rocks of the lithosphere. The ratio Ce^{+4}/Ce^{+3} reflects the "oxidation" degree of the zircon (and rock) formation and Eu^{+3}/Eu^{+2} – "reducing" properties of the source which allows one to control the level of the oxygen fugacity. A correlation of the ratio Ce^{+4}/Ce^{+3} in zircons ("geochemical buffer" – "CeB") and petrological buffer FMQ of rocks in the lithosphere vertical section has been performed. This allows one to determine the boundaries of the "upper" and "lower" parts of the lithosphere and reveal the similarity of the variation range of the oxygen fugacity in the upper lithosphere and analogous parameters of the crustal rocks of different age. Besides it helps to establish unique reducing parameters for oxygen in the foot part of the lithosphere.

Аннотация. В статье представлены вариации отношений Ce^{+4}/Ce^{+3} и Eu^{+3}/Eu^{+2} в цирконах из различных мантийных пород литосферы. Отношение Ce^{+4}/Ce^{+3} отражает степень "окисленности" образования циркона (и породы), а Eu^{+3}/Eu^{+2} – "восстановительные" свойства источника, что позволяет контролировать уровень летучести кислорода. Проведена корреляция отношений Ce^{+4}/Ce^{+3} в цирконах ("геохимического буфера" – "CeB") с петрологическим буфером FMQ в вертикальном разрезе литосферы, что позволило определить границы "верхней" и "нижней" частей литосферы и выявить сходство диапазона вариаций летучести кислорода в верхней части литосферы с аналогичными параметрами пород коры разного возраста, а также установить уникально восстановительные параметры для кислорода в подошвенной части литосферы.

Key words: oxygen fugacity, mantle lithosphere, REE in zircons
Ключевые слова: летучесть кислорода, мантийная литосфера, редкоземельные элементы в цирконах

1. Introduction

A significant range for the variation of oxygen fugacity in the mantle rocks influences the redistribution of elements with varying valency (Fe, Eu, V, Cr, Ce, etc.) in the rocks, rock-forming and accessory minerals. The quantitative assessment of the oxygen data variation range has so far been constrained only by the application of the FMQ petrological buffer. The prospects for the application of other methods have not been implemented yet. This research demonstrates an effort to use rare-earth elements for the analysis of the oxidation-reduction setting evolution in the mantle rocks on the basis of Ce^{+4}/Ce^{+3} and Eu^{+2}/Eu^{+3} ratio evolution for the zircons of different genesis, and correlation with the petrological buffer.

2. Petrological regulation of the oxygen fugacity variations in the mantle

The FMQ pertological buffer (*Ballhaus*, 1993) was long ago suggested for the mantle rocks of various genesis occurring at different depths using the correlation between rock-forming and accessory minerals. The petrological buffer is a primary indicator that records fO_2 variations from +4 to -6 in $\Delta\log fO_2$. This corresponds to the trend of reduction in oxygen fugacity with increasing depth and temperature of the mantle lithosphere rocks (*Galimov*, 1998; *Kadik et al*., 1998; *Ashchepkov et al*., 2004; 2008; 2009; *Galimov*, 2005; *Kadik et al*., 2006; *Kadik*, 2006; *Glebovitsky et al*., 2009; *Ryabchikov, Kogarko*, 2009; *Ryabchikov et al*., 2009; *Ryabchikov*, 2009). The current model is based on the empirical and theoretical data, accounting for the most reducing conditions (with participation of H and C) in the deep zones of the mantle, and oxidizing (OH-, H_2O) in the upper lithosphere.

About 125 cross-sections of the lithosphere were calculated using the data for the kimberlite pipes in Yakutia, Africa, North America, and Baltics (*Ashchepkov et al*., 2004; 2008; 2009) on the basis of the FMQ buffer variations for oxygen. This is almost equivalent to the interval of the petrological scale for the thickness of the entire lithology of the lithosphere, confirming its vertical zoning. Table 1 shows an example of typical series of kimberlite pipes in Yakutia that cover the whole stratigraphy of the lithosphere. It includes ilmenite (***ilm***) and chromite (***chrom***), as well as inclusions of chromite in diamonds (***chr.inclu***) for which FMQ buffer calculations have been done. It is important that this research has supported the evidences for the lithosphere zoning for which seven to twelve horizons have been recorded in accordance with the thermobarometer data and

compositional variations of certain minerals. Besides, there are reasonably constant minimum values for oxygen fugacity found for the deepest peridotites, that are particularly common for the chromite inclusions in diamonds (-4 to -6.5 in accordance with the FMQ scale).

Table 1. Variation of FMQ values for fO_2 in the Yakutian kimberlites (*Ashchepkov et al.*, 2004; 2008; 2009)

Pipe	Region	Depth (kbar)	Mineral	FMQ Interval
Udachnaya	Yakutia	40-71	ilm	+0.5 // -2
		12-72	chrom	+1 // -3.5
		50-65	chr.inclu	-2 // -3.5
Mir	Yakutia	18-63	ilm	+0.5 // -2
		53-65	chrom	-2.0 // -5
		40-70	chr.inclu	-2 // -6
Sytykanskaya	Yakutia	20-65	ilm	-0.5 // -2.5
		20-75	chrom	0 // -4.5
		60-70	chr.inclu	-1.7 // -4
Aykhal	Yakutia	38-66	ilm	-0.2 // -1.6
		15-55	chrom	-1 // -3
		55-75	chrom	-1 // -6.5
		50-65	chr.inclu	-2 // -4
Komsomolskaya	Yakutia	27-65	ilm	-0.5 // 1.5
		50-65	chr.inclu	-2 // -4
Internationlnaya	Yakutia	40-65	ilm	-1 // -2
		15-67	chrom	0 // -6
		55-60	chr.inclu	-2 // -5

Thus, the calculated and actual data for the peridotites and mantle magmas definitely indicate variation in oxygen fugacity towards the predominance of reducing regimes at the deepest horizons of the lithosphere in the field of graphite and diamond stability (garrnet.facies).

These root zones are presently considered as relics of the oldest subcontinental depleted Archaean mantle (SCLM) (*Griffin et al*., 1999; 2003; 2004; *Pearson et al*., 1999; *Rubanova et al*., 2010, etc.). Similar geochronological interpretation reflects a trend in petrogenic evolution and rare elements ratios in the Archaean-Proterozoic-Phanerozoic series, and emphasizes compositional variations of younger mantle (mantle metasomatism, etc.) in the lower and upper parts of the mantle lithosphere. It is marked by appearance of eclogites (*Burgess et al*., 1992, etc.), pyroxenites, meimeichites, Siberian trapps (*Sobolev et al*., 2009, etc.). For the last-mentioned rocks, an increased fugacity in the FMQ buffer is recorded to be up to +2 and higher (*Ryabchikov et al*., 2009). In some publications, compositional changes of individual minerals (garnets, pyroxenes, etc.) have been observed, that was in many cases considered as results of flows from the asthenosphere. The FMQ buffer was also used for the rough estimation for the oxygen influence on the secondary processes of alteration of mafic rocks and peridotites in the upper parts of the lithosphere where the increased values in the FMQ buffer of 0 to +1.7 for the peridotitic xenoliths with the evidences of intense metasomatism (*Ballhaus*, 1993). The most interesting results were obtained for the granitization of the Belomorian Fm metagabbro-norites (*Khodorevskaya*, 2009) with increasing $\Delta \log fO_2$ in the FMQ buffer from -1 to +4. It is impossible to disregard the oxidizing (oxidation) effect related to the gradual crustal growth at the presence of the atmospheric oxygen, which is especially important due to the evolution of the organogenic component of the crust and atmosphere in geological time. This agrees with the increase of oxidation potential in the upper zones of the lithosphere, and does not contradict its total vertical zoning. However, secondary geochemical changes in the upper parts of the lithosphere are still poorly studied in comparison with the depth processes (*Griffin et al*., 2003, etc.) that is not clear. Still, issues of early differentiation and homogenization at the stages of condensation and Earth accretion, reasons for the evolution of mantle magma composition and generation in geological time, as well as other not directly related to the FMQ buffer remain open.

3. Application of rare-earth element geochemistry in zircons to the analysis of the lithosphere heterogeneity

Among accessory minerals of the lithosphere, zircons deserve a special attention since positive Ce and negative Eu anomalies in REE are typical of zircons. As it was earlier stated in (*Ballard et al*., 2002; *Balashov, Skublov*, 2009; 2011), two forms of valency (Ce^{+4} and Ce^{+3}) present as isomorphic admixture in the zircon

structures from the different rock types. This allowed suggesting that their ratio records an actual level of oxygen fugacity in the course of zircon generation, which should correspond to the petrological parameters of fO_2 in the initial melt or solution. However, direct evidences for the mantle rocks have not yet been published, but the possibility of such Ce separation in solutions was experimentally found for cerium (*Takahashi et al*., 2000). The calculation of data for Ce^{+4}/Ce^{+3} in zircons is published in (*Balashov, Skublov*, 2009; 2011). The Ce^{+4}/Ce^{+3} content and ratios were estimated in chondrite-normalized C1 (*McDonough, Sun*, 1995) data: $Ce^{+3}{}_n = 0.5 (La_n+Pr_n)$, $Ce^{+4}{}_n = Ce_n - Ce^{+3}{}_n$. The error with regard to the other types of calculation was on average 5 %, that falls within the error level when measuring other REE. For the Eu^{+2}/Eu^{+3} pair, the chondrite-normalized data were used, $Eu^{+3}{}_n = Eu^* = 0.5 \times (Sm_n + Gd_n)$, and $Eu^{+2}{}_n = Eu_n$. This research calculates Ce^{+4}, Ce^{+3}, Eu^{+3}, and Eu^{+2}, and variations of their ratios (Table 2) from the xenoliths of the Chromur pipe, peridotite xenoliths of N.China (*Zheng et al*., 2006) kimberlites of the Mir, Radiovolnovaya, Interkosmos, Podsnezhnaya, Orekhovaya, Aikkhal pipes, Anomalies SH-9, K-52, K-53, K-62, 163, Dianga, Skiper birigindit (Yakutia), Orapa, Dgvaneng (Botswana), Wesselton, Bultfonten, Sekameng, Mohae, De Biirs, Leisister, Monasteri, Noeniput, Dyke 170, Kimberley Pool (South Africa), Timber Creek (Australia), as well as for zircons from the Argayal lamproites (Australia), Kirovograd Block (Ukraine), and Panozero complex (Central Karelia) (*Belousova et al*., 1998; *Belousova*, 2000; *Yatsenko et al*., 2000; *Skublov et al*., 2009). Zircons from many of those localities are lower crustal xenocrysts! Before using the zircons for this study one should really filter the data to select ONLY the grains that have trace-element compostion defined for the mantle zircons (e.g., total REE less than 50 ppm, low U, Th, Y). These data describe zones of the mantle lithosphere at different depth levels to mainly correspond to the variation from 30 to 65-75 kbar at the corresponding growth of temperature (*Ashchepkov et al*., 2008; 2009).

This research was aimed at interpreting factors that define migration of rare and rare earth elements, as well as at revealing influence of volatiles (primarily of oxygen, and water) on genesis of mantle rocks and their further transformation, and at tracing the evolution of oxygen fugacity through geological time. Table 2 includes Ce^{+4}/Ce^{+3} and Eu^{+2}/Eu^{+3} ratios calculated by the authors as indices of oxidation/reduction degree for oxygen fugacity in the vertical sequence of the lithosphere. This seems to correspond to the directed reduction of Ce^{+4}/Ce^{+3} from 34.2 to 0.01, and increase for Eu^{+2}/Eu^{+3} from 0.02 to 7.13 towards the bottom of the lithosphere. This should correspond to the FMQ buffer related reduction of fO_2 from +4 to -6 in $\Delta\log fO_2$. This interval is quite thoroughly checked by numerous petrological studies, but within ±1, a value that is roughly one order stands worn towards Ce^{+4}/Ce^{+3}. This divergence was eliminated at the statistic processing of the initial data. It should be noted that the similarity of the Ce^{+4}/Ce^{+3} variation ranges for the zircons from various types of mantle rocks allowed joining the zircon data into Table 2. Alongside, since some zircons demonstrate low content of light lanthanoids (La, Ce and Pr) with no possibility of measuring Ce^{+4}/Ce^{+3} with certain accuracy, such data were taken from Table 2 into Table 3 since Eu^{+2}/Eu^{+3} ratios there reaches peak values for the zircons from the lower part of the lithosphere. Table 2 has a few shortcomings among which there is absence of certain connection of calculated data related to Ce^{+4}/Ce^{+3} to Eu^{+2}/Eu^{+3} with regard to PT parameters since these petrological data are inavailable for zircons. Exactly because of this, one should rely on quite approximate data of the value levels for the FMQ buffer (*Ballhaus*, 1993; *Kadik*, 2006, etc.) shown in Table 2 as per the total calculated range for this buffer.

Table 2. Variations of FMQ values for rocks and Ce^{+4}/Ce^{+3} and Eu^{+2}/Eu^{+3} ratios in zircons

Ce-4/3	FMQ	Eu-2/3	Rocks	Location	Region	Sample N
34.2	4.00	0.44	Peridotitic xen.	Haning Pr.	China	Y974-25
34	4.00	0.19	Peridotitic xen.	Haning pr. Pr.	China	Y971-5
27.3	3.83	0.35	Lamproite	Argyle	Australia	Arg-9
27.1	3.83	0.58	Lamproite	Argyle	Australia	Arg-10
26.2	3.83	0.28	Lamproite	Argyle	Australia	Arg-7
26	3.83	0.56	Basalt gravel	Elliston, SA	Australia	E-12-3-18
23.7	3.66	0.57	Lamproite	Argyle	Australia	Arg-9 rim
23	3.66	0.60	Chomur xen.	Chomur Kim.	Yakutia	Chromur-6
22.8	3.66	0.85	Chomur xen.	Chomur Kim.	Yakutia	Chromur-2
22.4	3.66	0.50	Lamproite	Argyle	Australia	Arg-8 rim
20.8	3.49	0.55	Lamproite	Panozero	C. Karelia	12,1-ign
20.5	3.49	0.74	Lamproite	Argyle	Australia	Arg-10 rim
20.2	3.49	0.46	Chomur xen.	Chomur Kim.	Yakutia	Chromur-7
20.1	3.49	0.44	Chomur xen.	Chomur Kim.	Yakutia	Chromur-3

19.8	3.32	0.39	Lamproite	Argyle	Australia	Arg-15
19.5	3.32	0.57	Chomur xen.	Chomur Kim.	Yakutia	Chromur-5
19.3	3.32	0.13	Peridotitic xen.	Haning province	China	Y974-30
19.1	3.32	0.02	Peridotitic xen.	Haning province	China	Y971-4c
18.4	3.15	0.62	Lamproite	Panozero com.	C. Karelia	12,2-ign
18.3	3.15	0.27	Basalt gravel	Elliston, SA	Australia	E12-2-49
16.7	3.15	0.62	Lamproite	Argyle	Australia	Arg-7 rim
16.4	2.98	0.81	Kimberlite	Ruslovaya	Russia	Ruslov-2A
16.1	2.98	0.47	Chomur xen.	Chomur Kim	Yakutia	Chromur-8
16	2.98	0.72	Kimberlite	Anomaly 50/	/6432	Orekh-2B
16	2.98	0.80	Lamproite	Argyle	Australia	Arg-8
16	2.98	0.40	Lamproite	Argyle	Australia	Arg-15 rim
16	2.98	0.32	Lamproite	Argyle	Australia	Arg-16 rim
15.7	2.98	0.68	Lamproite	Panozero comp.	C. Karelia	10,1-ign
15.1	2.81	0.65	Lamproite	Panozero comp.	C. Karelia	9.1 ign
14.8	2.81	0.25	Dolerite	Crimea Mount.	Ukraine	023/86-16
14.54	2.81	0.47	Lamproite	Argyle	Australia	Arg-18-3
14	2.81	0.25	Lamproite	Argyle	Australia	Arg-16
13.8	2.81	0.29	Lamproite	Argyle	Australia	Arg-17
13.1	2.64	0.59	Chomur xen.	Chomur Kimb	Yakutia	Chromur-1
13.1	2.64	0.19	Dolerite	Crimea Moun.	Ukraine	023/86-43
13	2.64	0.83	Kimberlite, Ye	Monastery Mine	S. Africa	An-K62-2B
12.7	2.47	0.57	Lamproite	Panozero comp.	C. Karelia	14,1-ign
12.67	2.47	0.17	Kimberlite	Aikhal xenolith	Yakutia	Aikhal-A
12.5	2.31	0.69	Kimberlite	Ruslovaya pipe	Russia	An50/6432-
12.3	2.31	0.94	Basalt gravel	Elliston, SA	Australia	E22-2-38
12	2.31	0.75	Kimberlite	Orekhovaya	Russia	1-V-b
11.7	2.14	0.78	Lamproite	Argyle	Australia	Arg-2
10.8	2.14	0.97	Kimberlite	Anomaly K-62	Yakutia	kn279(12)4
10.8	2.14	0.65	Lamproite	Panozero comp	C. Karelia	8,1-ign
9.82	1.97	0.30	Lamproite	Argyle	Australia	Arg-18-1
9.75	1.97	0.80	Kimberlite	Anomaly 50/	Yakutia	Orekh-1D
9.7	1.97	1.03	Kimberlite	Timber Creek	Australia	Radiovol.-
9.52	1.97	0.09	Lamproite	Kirovograd Bl	Ukraine	Kirov6/32-1
9.32	1.97	0.27	Lamproite	Argyle	Australia	Arg-18-2
9	1.80	0.75	Kimberlite, Ye	Monastery Mine	S. Africa	Interk.C.-c
9	1.80	0.07	Dolerite	Crimea Moun.	Ukraine	023/86-24
8.7	1.80	0.43	Lamproite	Argyle	Australia	Arg-17 rim
8.33	1.80	0.03	Lamproite	Kirovograd Bl.	Ukraine	kirov6/32-2
8.02	1.63	0.77	Kimberlite	Orekhovaya	Yakutia	An-K62-1B
7.71	1.63	1.13	Kimberlite	Radiovolnovaya	Yakutia	Jw16-core
7.67	1.63	0.92	Kimberlite	Interkosmos pipe	Yakutia	Dianga-2D
7.43	1.63	1.04	Kimberlite	Anomaly K-62	Russia	Orekh-1B
7.09	1.46	0.66	Lamproite	Panozero comp.	C. Karelia	1
7	1.46	0.15	Dolerite	Crimea Mount.	Ukraine	023/86-15
6.94	1.46	0.62	Kimberlite	Jwaneng	Botswana	Dianga-1B
6.87	1.46	1.05	Kimberlite	Dianga pipe	Yakutia	An-K65-1B
6.34	1.29	0.80	Kimberlite	Orekhovaya pipe	Yakutia	M103-2
6.11	1.29	0.84	Kimberlite	Dianga pipe, Yakutia	Russia	Dianga-1C
6.04	1.29	0.87	Kimberlite	Anomaly K-65	Russia	An-K65-1B

6	1.29	0.19	Dolerite	Crimea Mountains	Ukraine	023/86-45
5.99	1.29	0.16	Peridotitic xen.	Haning province	China	Y972-16
5.8	1.12	0.83	Kimberlite	Orekhovaya pipe	Yakutia	Orekh-1A
5.79	1.12	0.97	Kimberlite, Ye	Wesselton	S. Africa	M103-2
5.77	1.12	1.01	Kimberlite	Dianga pipe, Yakutia	Russia	Dianga-1C
5.76	1.12	0.70	Kimberlite	Orekhovaya pipe	Yakutia	Orekh-2A
5.75	1.12	1.07	Kimberlite	Wesselton	S. Africa	M103 2
5.72	1.12	0.97	Kimberlite	Anomaly 152	Yakutia	An152-A
5.7	0.95	0.59	Kimberlite	Jwaneng	Botswana	Jw3-rim
5.7	0.95	0.14	Dolerite	Crimea Mountains	Ukraine	023/86-2
5.6	0.95	0.28	Dolerite	Crimea Mountains	Ukraine	023/86-11
5.59	0.95	0.17	Lamproite	Argyle	Australia	Arg-4
5.44	0.95	0.78	Kimberlite	Anomaly 165	Yakutia	An-165-2A
5.3	0.78	0.14	Dolerite	Crimea Mountains	Ukraine	023/86-51
5.2	0.78	0.18	Dolerite	Crimea Mountains	Ukraine	023/86-10
5.18	0.78	0.40	Basalt gravel	Elliston, SA	Australia	E12-2-50
5.14	0.78	0.55	Kimberlite	Jwaneng	Botswana	Jw5-core
5.12	0.78	0.57	Kimberlite	Orekhovaya pipe	Yakutia	Orekh-1C
5	0.78	0.84	Kimberlite, Ye	Bultfontein	S. Africa	M102-1
5	0.78	0.16	Dolerite	Crimea Mountains	Ukraine	023/86-44
4.92	0.61	0.86	Kimberlite	Anomaly 163	Yakutia	An-163-1
4.8	0.61	0.17	Kimberlite	Aikhal xenolith	Yakutia	Aikhal-B
4.76	0.61	0.72	Kimberlite	Orapa pipe	Botswana	Orapa-6
4.62	0.44	0.93	Kimberlite	Bultfontein	S. Africa	M102 1
4.53	0.44	0.55	Kimberlite	Jwaneng	Botswana	Jw3-core
4.52	0.44	0.74	Kimberlite	Anomaly 165	Yakutia	An-165-1A
4.38	0.44	1.00	Kimberlite	Interkosmos pipe	Yakutia	Interk.-rim
4.21	0.27	0.15	Dolerite	Crimea Mountains	Ukraine	023/86-5
4.2	0.27	0.29	Kimberlite	Anomaly 152	Yakutia	An152-C
4.06	0.27	0.96	Kimberlite	Ruslovaya pipe	Russia	Ruslov-2C
4.04	0.27	0.77	Dolerite	Crimea Mountains	Ukraine	023/86-7
4	0.27	1.10	Kimberlite	Sekameng/Buth But	S. Africa	M31 2
3.92	0.10	0.10	Dolerite	Crimea Mountains	Ukraine	023/86-37
3.88	0.10	0.16	Dolerite	Crimea Mountains	Ukraine	023/86-26
3.8	0.10	1.00	Basalt gravel	Elliston, SA	Australia	E22-2-37
3.69	-0.07	0.94	Kimberlite, Ye	Kao 1	S. Africa	M42(2)4
3.56	-0.07	0.35	Basalt gravel	Elliston, SA	Australia	E-12-3-21
3.52	-0.07	0.12	Lamproite	Kirovograd Block	Ukraine	kirov-3/17-3
3.46	-0.07	0.98	Kimberlite, Ye	Wesselton	S. Africa	M103-1
3.44	-0.07	0.63	Kimberlite	Anomaly 165	Yakutia	An-165-1B
3.4	-0.24	0.85	Kimberlite, BL	Mothae	S. Africa	M30(10) 1
3.37	-0.24	0.29	Dolerite	Crimea Mountains	Ukraine	023/86-14
3.36	-0.24	0.93	Kimberlite	Mothae	S. Africa	M30(9) 2
3.31	-0.24	0.85	Kimberlite	Anomaly K-52	Yakutia	AnK52-A rim
3.24	-0.41	0.65	Lamproite	Panozero complex	C. Karelia	7,1-M
3.23	-0.41	0.88	Kimberlite	De Beers Mine	S. Africa	M101 3
3.18	-0.41	0.21	Basalt gravel	Elliston, SA	Australia	E20-1-27
3.12	-0.58	0.36	Kimberlite	Timber Creek, NT	Australia	11-Y-t
3.11	-0.58	0.83	Kimberlite, BL	De Beers Mine	S. Africa	M101-3
3.07	-0.58	0.85	Kimberlite	Ruslovaya pipe	Yakutia	Ruslov-1B

3	-0.58	0.63	Kimberlite, Ye	Monastery Mine	S. Africa	ROM-179-2
3	-0.58	0.85	Kimberlite	Anomaly K-53	Yakutia	An-K53-2A
2.9	-0.58	0.51	Kimberlite	Chomur xenolith	Yakutia	Chromur=4
2.87	-0.75	0.48	Kimberlite	Jwaneng	Botswana	Jw16-rim
2.87	-0.75	0.08	Lamproite	Kirovograd Block	Ukraine	kirov-2/30
2.84	-0.75	0.20	Lamproite	Argyle	Australia	Arg-5
2.7	-0.92	0.70	Kimberlite, BL	Monastery Mine	S. Africa	ROM-179-1
2.7	-0.92	0.74	Lamproite	Panozero complex	C. Karelia	13,1-M
2.62	-0.92	1.10	Kimberlite	Leicester	S. Africa	Leic-7 rim
2.54	-1.08	0.26	Dolerite	Crimea Mountains	Ukraine	023/86-39
2.52	-1.08	1.07	Kimberlite	Mir pipe	Yakutia	Mir-core-1
2.49	-1.08	0.56	Kimberlite	Anomaly K-52	Yakutia	An K52-B
2.45	-1.08	1.24	Kimberlite	Anomaly K-62	Yakutia	An-K62-1A
2.43	-1.08	1.02	Kimberlite	Podsnezhnaya pipe	Yakutia	Podsn.-1B
2.33	-1.25	0.12	Dolerite	Crimea Mountains	Ukraine	023/85-4
2.31	-1.25	1.03	Kimberlite	Monastery	S. Africa	Z-006-2
2.3	-1.25	0.88	Kimberlite	Orapa pipe	Botswana	Orapa-7
2.21	-1.42	1.05	Kimberlite	Anomaly K-65	Yakutia	An-K-65-1A
2.2	-1.42	1.56	Kimberlite, BL	De Beers Mine	S. Africa	M101-2
2.2	-1.42	0.77	Basalt gravel	Dobe Lead, NSW	Australia	Dobe-4
2.16	-1.42	0.89	Kimberlite	Skiper birigindite	Yakutia	Skiper
2.14	-1.42	0.89	Basalt gravel	Elliston, SA	Australia	E22-2-39
2.1	-1.59	0.74	Kimberlite, Ye	Lemphane	S. Africa	M27-1
2.08	-1.59	0.07	Lamproite	Kirovograd Block	Ukraine	kirov-1/29
2.04	-1.59	1.01	Kimberlite	Noeniput	S. Africa	m32 4
2	-1.76	0.66	Kimberlite, BL	Kao 1	S. Africa	M42(2) 3
2	-1.76	0.78	Basalt gravel	Dobe Lead, NSW	Australia	Dobe-5
1.94	-1.76	0.88	Kimberlite	Anomaly K-52	Yakutia	An K52-Ac
1.94	-1.76	0.13	Lamproite	Kirovograd Block	Ukraine	kirov4/25-5
1.87	-1.93	0.81	Basalt gravel	Dobe Lead, NSW	Australia	Dobe-6
1.86	-1.93	0.07	Lamproite	Kirovograd Block	Ukraine	kirov-6-32-3
1.84	-1.93	0.08	Lamproite	Kirovograd Block	Ukraine	kirov-7/32-3
1.82	-2.10	0.90	Kimberlite	Noeniput	S. Africa	M32 3
1.8	-2.10	0.17	Lamproite	Kirovograd Block	Ukraine	kirov-4/25-3
1.8	-2.10	0.22	Dolerite	Crimea Mountains	Ukraine	023/86-12
1.75	-2.27	1.06	Kimberlite	Anomaly K-62	Yakutia	An-K62-2A
1.73	-2.27	0.88	Kimberlite	Monastery	S. Africa	MZR-Z-026-1
1.71	-2.27	0.62	Basalt gravel	Elliston, SA	Australia	E21-1-30
1.7	-2.27	1.22	Kimberlite	Anomaly K-53	Yakutia	An-K53-1A
1.67	-2.27	1.19	Kimberlite	Bultfontein	S. Africa	M102 2
1.67	-2.27	0.35	Dolerite	Crimea Mountains	Ukraine	023/86-18
1.64	-2.44	0.22	Kimberlite	Timber Creek	Australia	2-V-b
1.64	-2.44	0.93	Kimberlite, Ye	DYKE 170	S.Africa	M 28(8)2
1.63	-2.44	0.92	Kimberlite	Mir pipe	Yakutia	Mir-rim-7
1.63	-2.44	0.14	Lamproite	Kirovograd Block	Ukraine	kirov-5-1
1.62	-2.44	1.08	Kimberlite, Ye	Bultfontein	S. Africa	M102-2
1.58	-2.61	0.96	Kimberlite	Orapa pipe	Botswana	Orapa-8
1.57	-2.61	0.18	Lamproite	Kirovograd Block	Ukraine	kirov-4/25-2
1.42	-2.78	0.55	Kimberlite	Monastery	S. Africa	ROM-121
1.37	-2.78	0.85	Kimberlite, BL	Monastery Mine	S. Africa	ROM-179-3

1.32	-2.78	1.00	Kimberlite	Mir pipe	Yakutia	Mir-rim-9
1.29	-2.78	0.53	Lamproite	Panozero complex	C. Karelia	3,1-MM
1.29	-2.78	0.09	Lamproite	Kirovograd Block	Ukraine	kirov-4/25-1
1.19	-2.95	1.15	Kimberlite	Leicester	S. Africa	Leic-7core
1.18	-2.95	0.97	Kimberlite	Mothae	S. Africa	M30(10) 4
1.15	-2.95	1.16	Kimberlite	Mothae	S. Africa	M30(10) 2
1.13	-2.95	0.68	Kimberlite	Orapa pipe	Botswana	Orapa-4
1.09	-3.12	0.96	Kimberlite	Monastery	S. Africa	MZ-05-1
1.06	-3.12	0.79	Kimberlite	Dyke 170	S. Africa	M28(4) 2
1.04	-3.12	0.23	Peridotitic xen.	Haning province	China	Y971-7
0.99	-3.29	1.17	Kimberlite	Bultfontein	S. Africa	M102 3
0.96	-3.29	1.17	Kimberlite	Monastery	S. Africa	Z-012-1
0.96	-3.29	1.10	Kimberlite	Kimberley Pool	S. Africa	M104 3
0.95	-3.29	1.04	Kimberlite, BL	Mothae	S. Africa	M30(10) 2
0.94	-3.29	2.21	Kimberlite	Timber Creek	Australia	20-O
0.93	-3.29	0.24	Lamproite	Kirovograd Block	Ukraine	kirov-6/32-4
0.91	-3.29	0.94	Kimberlite	Mothae	S. Africa	M30(9) 3
0.89	-3.46	1.00	Kimberlite	Jwaneng	Botswana	Jw13-rim
0.87	-3.46	0.74	Kimberlite	Mir pipe	Yakutia	Mir-core-2
0.87	-3.46	0.10	Lamproite	Kirovograd Block	Ukraine	kirov-5-2
0.86	-3.46	0.57	Kimberlite	Jwaneng	Botswana	Jw5-rim
0.86	-3.46	1.03	Kimberlite	Timber Creek, NT	Australia	11-Y-b
0.85	-3.63	0.52	Kimberlite	Timber Creek, NT	Australia	4-V-b
0.85	-3.63	0.89	Kimberlite	Timber Creek, NT	Australia	20-O-b
0.83	-3.63	0.80	Kimberlite	Mir pipe	Yakutia	Mir-rim-8
0.76	-3.80	1.28	Kimberlite	Orapa pipe	Botswana	Orapa-2
0.67	-3.80	2.28	Kimberlite, BL	Kao 1	S. Africa	M42(2) 1
0.67	-3.80	0.86	Lamproite	Panozero complex	C. Karelia	3,3-MMM
0.65	-3.80	0.94	Kimberlite	Mir pipe	Yakutia	Mir-core-3
0.65	-3.80	1.86	Kimberlite	Monastery	S. Africa	Z-067-2
0.58	-3.97	0.83	Kimberlite	Mir pipe	Yakutia	Mir-rim-6
0.58	-3.97	1.01	Kimberlite, Ye	Lemphane	S. Africa	M27-3
0.5	-4.14	0.80	Kimberlite	Anomaly 155	Yakutia	An-155-1B
0.49	-4.14	0.87	Kimberlite, BL	Mothae	S. Africa	M30(10) 3
0.48	-4.31	0.89	Kimberlite	Dyke 170	S. Africa	M28(4) 3
0.48	-4.31	0.85	Lamproite	Panozero complex	C. Karelia	3,2-MM
0.44	-4.31	0.84	Kimberlite, Ye	Monastery Mine	S. Africa	kn279(12)1
0.4	-4.47	1.19	Kimberlite	Monastery	S. Africa	Z-001-2
0.38	-4.47	0.93	Kimberlite	Mir pipe	Yakutia	Mir-rim-4
0.34	-4.47	1.06	Kimberlite	Monastery	S. Africa	Z-008-2
0.34	-4.47	0.88	Kimberlite	Monastery Mine	S. Africa	KN279(12) 1
0.27	-4.64	1.21	Kimberlite	Timber Creek	Australia	5-V-t
0.26	-4.64	0.81	Kimberlite	Anomaly Sh-9	Yakutia	An Sh9-A
0.25	-4.64	0.83	Kimberlite	Jwaneng	Botswana	Jw12-core
0.23	-4.81	0.15	Kimberlite	Kirovograd Bl.	Ukraine	kirov-3/17-2
0.23	-4.81	3.85	Kimberlite	Timber Creek	Australia	3-V-t
0.23	-4.81	0.13	Lamproite	Kirovograd Block	Ukraine	kirov=3/17-2
0.21	-4.98	0.80	Lamproite	Panozero complex	C. Karelia	1,1-MM
0.2	-4.98	1.03	Kimberlite	Jwaneng	Botswana	Jw12-rim
0.19	-4.98	1.03	Kimberlite	Jwaneng	Botswana	Jw13-core

0.19	-4.98	0.69	Basalt gravel	Inverell, NSW	Australia	Inverell-19
0.16	-4.98	0.78	Kimberlite, Ye	Kao 1	S. Africa	M42(2)2
0.13	-5.15	0.36	Kimberlite	Mir pipe	Yakutia	Mir-rim-5
0.13	-5.15	0.70	Kimberlite	Leningrad pipe	Yakutia	Leningr-A
0.12	-5.15	0.80	Kimberlite	Leicester	S. Africa	Leic-1
0.11	-5.15	0.96	Lamproite	Kirovograd Block	Ukraine	kirov-3/17-1
0.1	-5.32	0.95	Kimberlite	Orapa pipe	Botswana	Orapa-10
0.1	-5.32	0.93	Kimberlite, BL	Lemphane	S. Africa	M27-2
0.1	-5.32	1.74	Kimberlite	Monastery	S. Africa	Z-113-2
0.1	-5.32	0.93	Kimberlite, BL	Lemphane	S. Africa	M27-2
0.086	-5.32	1.45	Kimberlite	Monastery	S. Africa	MZ-06-2
0.06	-5.49	0.78	Kimberlite	Monastery	S. Africa	ROM-182-fl
0.06	-5.49	0.07	Lamproite	Kirovograd Block	Ukraine	Kirov-4/25-4
0.057	-5.49	1.29	Kimberlite	Monastery	S. Africa	Z-008-3
0.042	-5.66	1.31	Kimberlite	Monastery	S. Africa	Z-074-1
0.037	-5.66	1.03	Kimberlite, BL	Butha Buthe	S. Africa	M31-2
0.032	-5.83	0.53	Kimberlite	Orapa pipe	Botswana	Orapa-9
0.024	-5.83	0.92	Kimberlite	Orapa pipe	Botswana	Orapa-3
0.024	-5.83	0.92	Kimberlite	Orapa pipe	Botswana	Orapa-5
0.02	-6.00	0.69	Kimberlite	Orapa pipe	Botswana	Orapa-1
0.017	-6.00	0.67	Kimberlite, BL	De Beers Mine	S. Africa	M101-1
0.01	-6.00	2.70	Kimberlite, BL	DYKE 170	S. Africa	M28(8) 1
0.01	-6.00	3.45	Kimberlite, BL	SEKAMENG	S. Africa	M31-1

BL – Blue (Ign.?), Ye – Yellow (MM?). Ign – igneous MM – secondary zircon Ce4/3 = $\mathbf{Ce^{+4}/Ce^{+3}}$, Eu 2/3 = $\mathbf{Eu^{+2}/Eu^{+3}}$, FMQ buffer validation is shown below (=Δlog fO_2).

Table 3. Negative Ce^{+4}/Ce^{+3} values (?) and peak Eu^{+2}/Eu^{+3} in zircons of the deep lithosphere-related mantle rocks

Ce4/3	Eu2/3	Rocks	Location	Region	N Sample
-0.04	0.28	Dolerite	Crim Moun.	Ukraine	023/86-6
-0.06	0.62	Basalt gr.	Inverell, NSW	Australia	Inverell-21
-0.08	1.22	Kimberlite	Kao Quarry area	S. Africa	M41 3
-0.11	1.51	Kimberlite	Monastery	S. Africa	MZ-04-3
-0.13	1.33	Kimberlite	Monastery	S. Africa	MZ-05-2
-0.13	1.59	Kimberlite	Mothae	S. Africa	M30(9) 4
-0.16	0.8	Kimberlite	Monastery	S. Africa	MZR-Z-026-2
-0.21	1.6	Kimberlite	Monastery	S. Africa	Z-059-2
-0.32	0.52	Lamproite	Panozero	Karelia	2,1-MM
-0.35	0.71	Kimberlite	S Afr., Kao 1	S. Africa	M42(6) 6
-0.35	1.93	Kimberlite	Monastery	S. Africa	Z-001-4
-0.37	3.94	Kimberlite	Monastery	S. Africa	Z-074-2
-0.37	7.13	Kimberlite	Monastery	S. Africa	Z-011-1
-0.39	5.71	Kimberlite	Kao Quarry area	S. Africa	M41 4
-0.4	2.36	Kimberlite	Dyke 170	S. Africa	M28(7) 2
-0.41	2.75	Kimberlite	Monastery	S. Africa	Z-012-2
-0.51	1.82	Kimberlite	Monastery	S. Africa	Z-001-3
-0.53	0.91	Kimberlite	S Afr., Kao 3	S. Africa	M42(6) 8
-0.76	0.87	Kimberlite	S Afr., Kao 2	S. Africa	M42(6) 7

Ce4/3 = $\mathbf{Ce^{+4}/Ce^{+3}}$, Eu 2/3 = $\mathbf{Eu^{+2}/Eu^{+3}}$, FMQ buffer validation is shown below (=Δlog fO_2).

4. Regional geochemical features of zircon REE and Y distribution

It is necessary to remind that there are papers published about rare and rare earth element distribution in zircons (*Belousova et al.*, 1998; 2002; *Hoskin et al.*, 2000) where it was pointed at a need to account for the difference in the concentration of these elements from various mantle and crustal rock types. Moreover, by the example of the zircons from the South African kimberlites (Table 4), a clear, but slight division into two types (Table 4: Yellow and Bluish – cathodoluminescence images of kimberlitic zircons) in the concentrations of Ce, Y, Th and Th/U under relative stability of Hf (*Belousova et al.*, 1998), was noted.

Table 4. Some rare elements of zircons from different rocks

Region	Ce, ppm	Ce4/3	Y, ppm
Peridotit xenolites	32.6-3.2	39-1.04	1933-572
All Kimberlites	79-0.36	17.4-0.01	836-5.1
Yellow Kim., S. Africa	4.1-1	13-0.16	75-21
Bluish Kim., S. Africa	2.6-1	3.4-0.01	51-10.7
All Kim., Yakutia	23-0.7	17.4-0.13	778-6.2

One may assume (Fig. 1) that the South African zircons reflect regional features in rare element content. In this case, there is a reason for searching for similar criteria in other areas. It is true that Yakutian zircons demonstrate quite abrupt variations in Y concentrations (Fig. 2 and 3) among which there are zircons extremely enriched with Y (e.g., 778-341 ppm for the Orekhovaya and Skriper pipes) and with low Y content (42.7-6.2 ppm for the Mir pipe). Relative Hf stability (0.6-2 wt %) is thus clear at distinctly decreasing Ce^{+4}/Ce^{+3} ratio. Th/U stability with regard to Ce^{+4}/Ce^{+3} should also be noted (Fig. 4). Many researches suppose that zircons in kimberlites are not primary. In this case, one should believe that significant variations of rare elements favour such ideas. Although, the age, source, and regional structural features of the lithosphere should be taken into consideration. At the same time, peculiar variation of Ce^{+4}/Ce^{+3} ratio should be noted against the background of changes in other rare element concentrations.

In this section, it is appropriate to remind that the isotope-geochemical data allow dividing kimberlites at least into 3 types in terms of source from a depleted (MORB) and enriched (two levels of continental type) mantle (*Smith*, 1983; *Bogatikov et al.*, 2007, etc.) which have not yet been divided at the petrological FMQ scale since the location of MORB sources is strictly not defined in the scheme of vertical lithosphere zoning. The reasons of the isotope-geochemical contrast existence for these sources are still to be established.

This sends us back to the issue of emerging geochemical heterogeneity in the formation history of geochemical heterogeneity in the upper mantle that, most probably, is related to the earliest stages of the Earth's accretion. This is still to be interpreted.

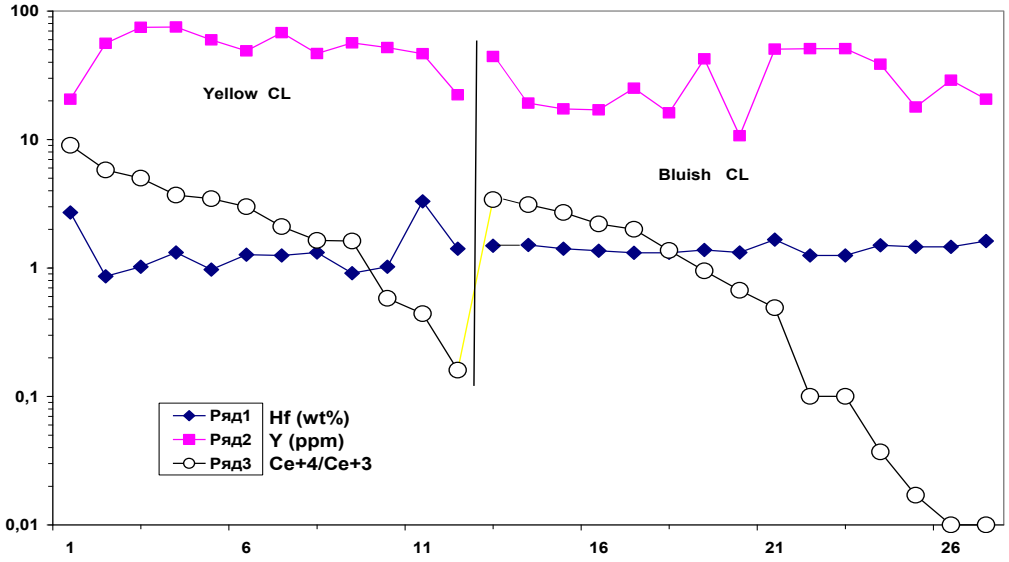

Fig. 1. Zircons of kimberlites from S. Africa

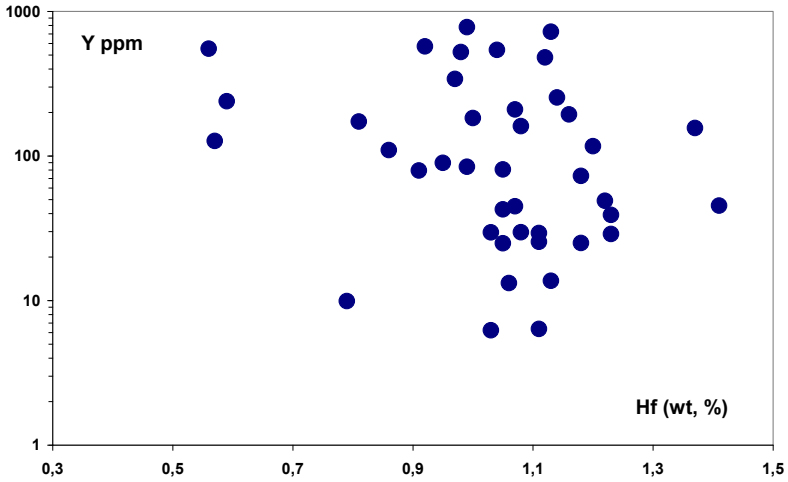

Fig. 2. Zircons of kimberlites from Yakutia

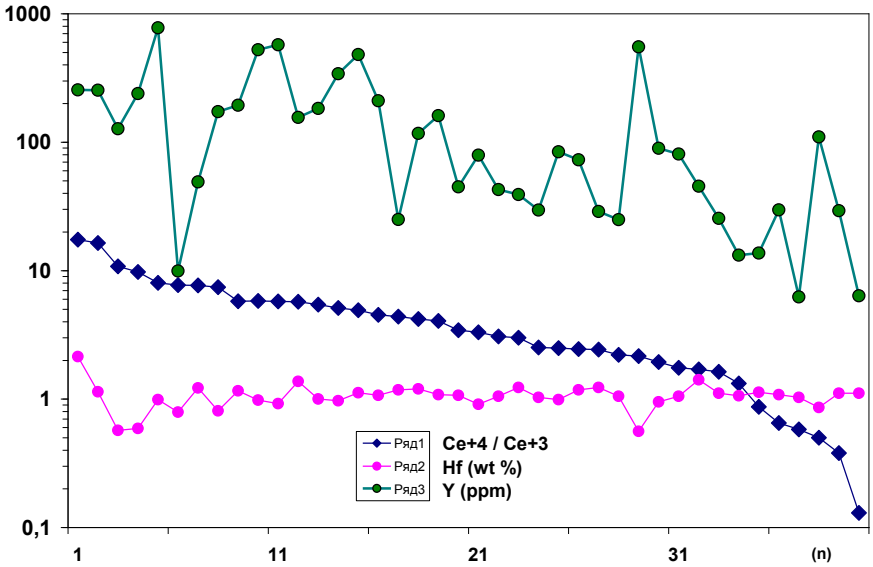

Fig. 3. Abundance of Hf, Y and Ce^{+4}/Ce^{+3} in zircons from the Yakutian kimberlites (*n* for the number of analyses)

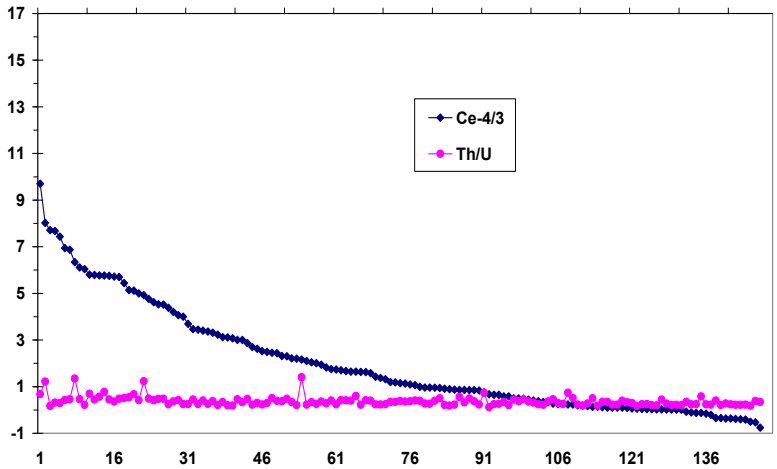

Fig. 4. Ce^{+4}/Ce^{+3} and Th/U ratios in the kimberlitic zircons

5. Variations in Ce^{+4}/Ce^{+3} and Eu^{+2}/Eu^{+3} ratios in zircons of the mantle lithosphere rocks

The statistics (Table 2 and 3, Fig. 5-7) shows that the Ce^{+4}/Ce^{+3} ratios in the kimberlites vary from 0.01 to 16.4, in the lamproites from 0.01 to 27.3, and in the basalt-dolerite from 0.01 to 26. The analogy is obvious in the behaviour of cerium fractionation. The sharply increased ratios that agree with the optimal oxidation in oxygen are significantly shifted to the level close to the crustal formations, or to the upper zones of the mantle lithosphere. On the contrary, minimum ratios indicate a negligible fraction of Ce^{+4} in zircons. This definitely testifies a sharply reducing setting of their generation. Such an interpretation strictly corresponds to the modern petrological schemes of the lithosphere vertical zoning based on the generalization related to the FMQ buffer (*Ashchepkov et al*., 2004; 2008; 2009; *Kadik*, 2006, etc.).

This should be supplemented with the fact that in the lower lithosphere Ce^{+4}/Ce^{+3} ratios sometimes can be negative. It may most probably be caused by analytical errors in the measurement of light lanthanoids due to their low content in zircons. This does not change conclusion on a sharply reduced concentration for Ce^{+4} in the lower parts of the lithosphere that agrees with the remaining REE data for this zone.

In general, significant Ce^{+4}/Ce^{+3} variations in the kimberlites, lamproites, and basalts indicate clear dependence on the variations of the redox zircon generation settings in the vertical section of the lithosphere that agrees with the above-stated petrological reconstructions (*Galimov*, 1998, etc.). It definitely indicates a probability of correlation in Ce^{+4}/Ce^{+3} variations with petrological buffers.

The Eu^{+2}/Eu^{+3} ratio in zircons is especially interesting since it reflects the degree of natural mantle or crustal system reduction state that actually corresponds to the oxygen fugacity and can be used for petrological reconstructions. Table 2 and 3 and Figs 5-7 show that in mantle rocks, Eu^{+2}/Eu^{+3} ratios in zircons predominantly vary within a tight range, i.e. from 7.13 to 0.15 in kimberlites, from 0.96 to 0.03 in lamproites, and from 1.00 to 0.07 in basalts. The maximum ratios are recorded in zircons from deeper parts of the lithosphere if we focus on synchronous minimum values for Ce^{+4}/Ce^{+3}. Proceeding from the general petrological scheme of the vertical oxygen fugacity zoning, minimum Eu^{+2}/Eu^{+3} values should be observed in the uppermost parts of the lithosphere while the maximum ones are at the bottom where Eu^{+2} should dominate. This effect was actually observed in some zircons. Such abnormal variation agrees with the reverse trend for Ce^{+4}/Ce^{+3}. Figs 5-7 demonstrate a strict compliance with exactly this regularity for mantle rocks. It is also obvious that the Ce data are more informative than the Eu results. In the deep-seated horizons of kimberlites in the lithosphere, there are sections with a sharply increased Eu^{+2}/Eu^{+3} ratio, which also agrees with the petrological conclusions on expecting such a oxygen fugacity regime under the conditions of a sharp deficiency in water at the excess of hydrogen (*Galimov*, 1998; *Kadik*, 2006, etc.).

Thus, joint information on varying Ce^{+4}/Ce^{+3} and Eu^{+2}/Eu^{+3} ratios can be considered as an individual geochemical substantiation of present heterogeneity in the lithosphere.

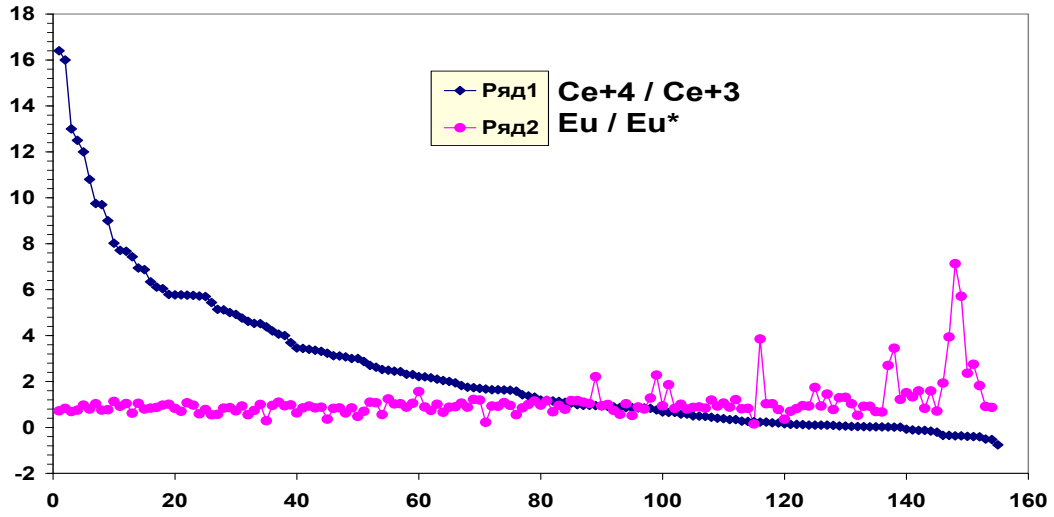

Fig. 5. Contrasting variation of Ce^{+4}/Ce^{+3} and Eu^{+2}/Eu^{+3} in zircons from the kimberlites (0-155 = *n*)

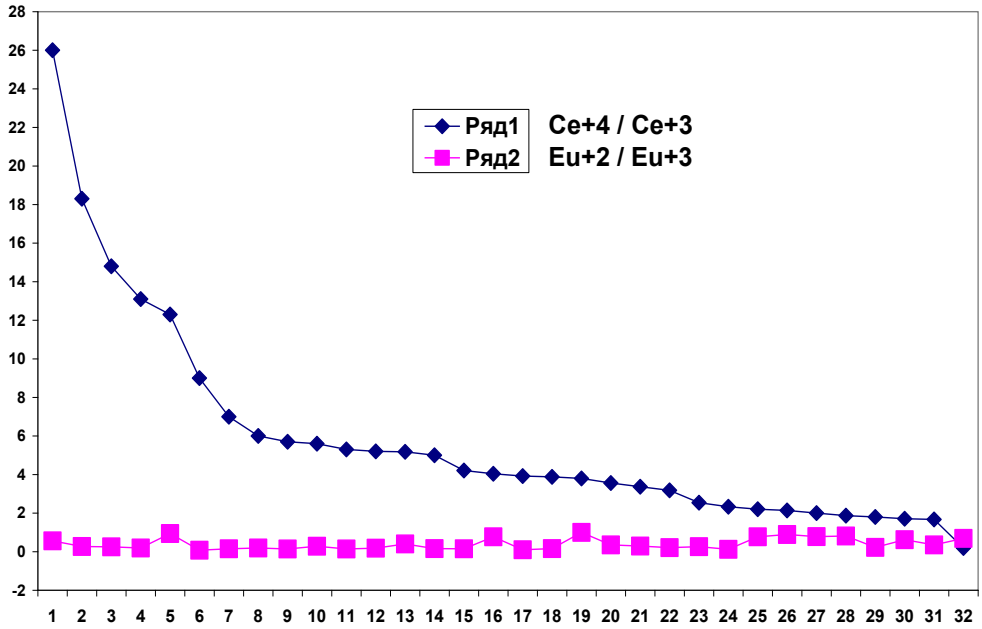

Fig. 6. Contrasting Ce^{+4}/Ce^{+3} and Eu^{+2}/Eu^{+3} variations in zircons from the lamproites (1-32 = *n*)

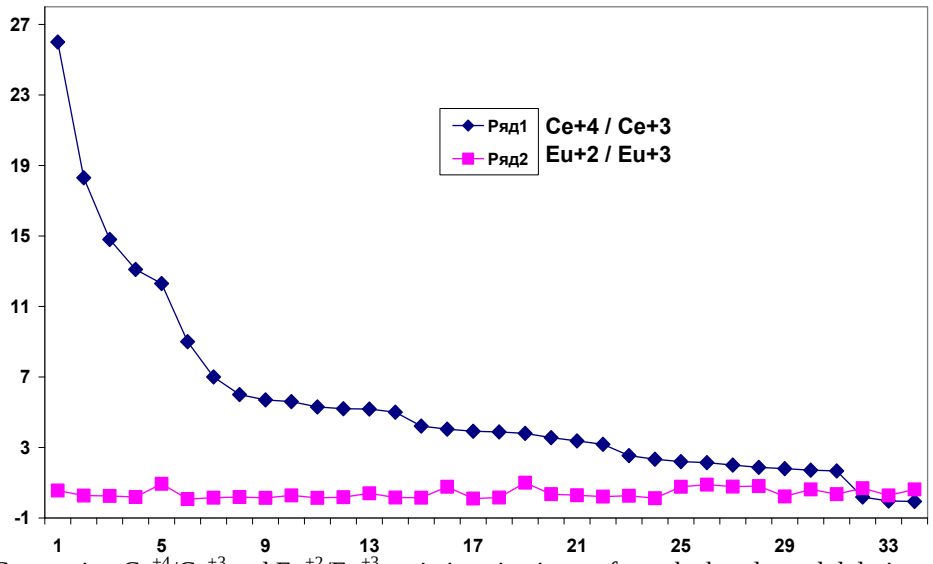

Fig. 7. Contrasting Ce^{+4}/Ce^{+3} and Eu^{+2}/Eu^{+3} variations in zircons from the basalts and dolerites (1-34 = *n*)

6. High Ce^{+4}/Ce^{+3} ratios in zircons of the upper lithosphere

It seems that the whole zircon recrystallation data with an abrupt increase of Ce^{+4}/Ce^{+3} ratio, that has probably agreed with secondary zircons. Highly increased ratios are also recorded in alkaline rocks and pertinent zircons (Fig. 8, and 9). It is also marked in crustal contamination (*Balashov et al*., 2010) in the upper levels of the mantle or the stage of mantle-core interaction.

What stands out is the intensity of the varying Ce^{+4}/Ce^{+3} ratio that exceeds four orders. Such a range is unique in the degree of variation and maximum in the level of Ce^{+4}/Ce^{+3}. For example, for the peridotitic xenoliths from the Chromur lamproite, the Ce^{+4}/Ce^{+3} ratio varies from 23 to 2.9, for the syenitic pegmatites from Norway, the Ce^{+4}/Ce^{+3} ratio varies from 506 to 149, and for the mantle carbonatites in Kovdor, from 1.36 to 0.14. Along with this, in some cases, a reverse situation is observed when the secondary zircons record a reducing oxygen fugacity (*Balashov, Skublov*, 2011). It probably agrees with a range of processes in igneous and secondary zircons within the crust.

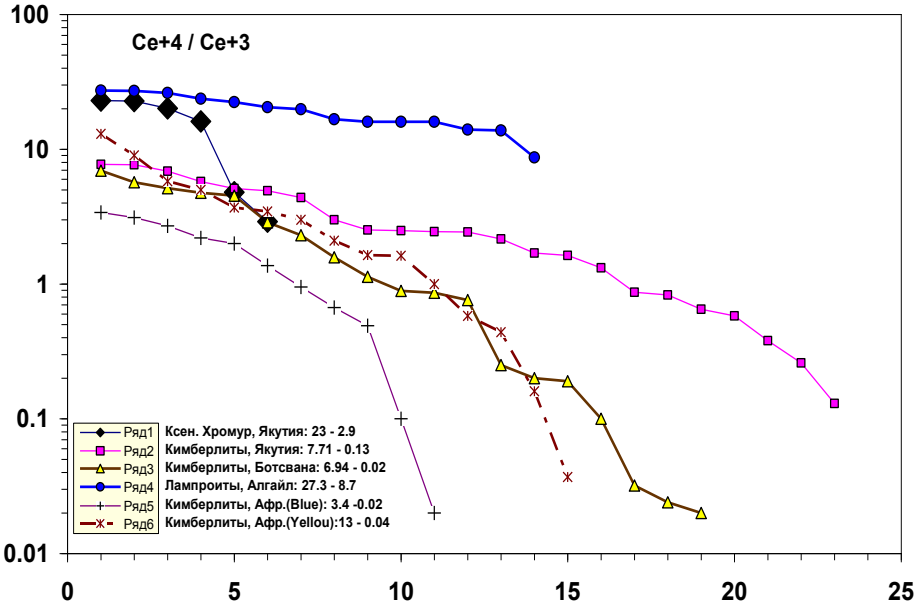

Fig. 8. Varying Ce^{+4}/ Ce^{+3} ratio in zircons from certain kimberlites and lamproites as a reflection of initial igneous processes and superimposed (secondary) transformation. The initially igneous and secondary zircons (Blue and Yellow) for the certain pipes in South Africa were earlier calculated (*Belousova et al*., 1998). (0-25 = *n*)

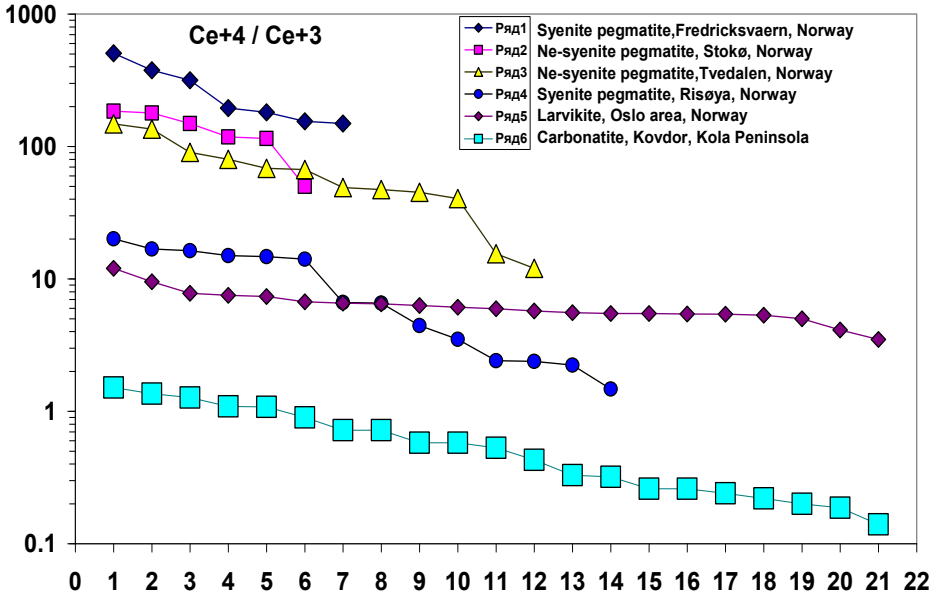

Fig. 9. Ce^{+4}/Ce^{+3} variations in zircons of the alkaline rocks and pegmatites (0-22 = *n*)

7. Oxygen fugacities correlation between its normalize to FMQ buffer rocks and Ce^{+4}/Ce^{+3} ratio of zircons

The easiest way to correlate FMQ data and varying Ce^{+4}/Ce^{+3} ratio can be represented as a result of direct dependence on a single factor, the oxygen fugacity (Table 2). The FMQ data suggests that the oxygen fugacity is roughly recorded within the interval of -6 to +4 in $\Delta \log fO_2$. Ce^{+4}/Ce^{+3} data from Tables 2 and 3 taken as conventional "CeB" – "geochemical buffer" can be distinguished in rock types:

in kimberlite from 0.01 to 16.4 (n = 155);
in lamproite from 0.01 to 27.3 (n = 51);
in peridotitic xenoliths from 1.04 to 34.3 (n = 16);
in basalts and dolerite from 0.01 to 26 (n = 33).

In spite of the difference in the number of analyses, author's materials, and possible variations in the accuracy of the analysis, quite similar limits of varying Ce^{+4}/Ce^{+3} ratio in zircons (for the geochemical buffer further on we have used a range of 34 to 0.01) are observed for the petrological types of rocks concerned. This includes aggregate differencies with increased values in CeB (probably contaminated by crustal components or asthenosphere additive with varying composition).

Therefore, there are two individual oxygen fugacity measurement systems for the lithosphere with clear uncertainty for the correlation between them. It would seem that there is a way out if average estimations for the both buffers for the lithosphere would have been known. However, it is absent since the zero value in the FMQ buffer only reflects the upper limit of the unaltered mantle peridotites. But this is only relative since the field around 0±1 is filled with slightly and heavily altered peridotites (*Ballhaus*, 1993). Moreover, the estimation of the average value for the principal mass of primitive peridotites tends to the FMQ area with parameters from 0 to -3 to correspond to the shift towards iron-wustite balance... It is worth reminding that, for the mantle zircons from the rocks of different age partially affected by secondary, exactly this shift is recorded (*Kadik et al*., 1998). Moreover, for the garnet ultramafic xenoliths from the kimberlites of South Africa, in the fields of graphite – diamond, a shift of $\Delta\log fO_2$ in the FMQ buffer is found to be 1.9-2.4 times and more (*McCammon et al*., 2001). Thus, reduced fugacity definitely records average mantle oxygen ratios between the initial and altered rocks. With due regard of the abovestated, we have tried to use different ways of estimations based on the total range of data on both buffers that cover the whole thickness of the lithosphere: {lower boundary ~75 kbar; Ce^{+4}/Ce^{+3} = 0.01 and Log = -2; FMQ = -6; upper boundary ~15 kbar; Ce^{+4}/Ce^{+3} = 34.3 and Log = 1.535; FMQ =+4}.

For the initial calculation of the aggregate data (Table 2) on varying Ce^{+4}/Ce^{+3} ratios were preliminary divided into 60 statistically homogenous groups (*Rodionov*, 1968) to completely cover the whole range of the FMQ variations. Using methods of regressive analysis for the data analysis within the space of CeB – FMQ buffer parameters allowed obtaining the following results. The dependence between the logarithms of Ce^{+4}/Ce^{+3} to base 10, and calculated values in the FMQ buffer is described at the chosen significance level of 0.01 by the 4th degree polynomial (Fig. 10):

$$Log_{10}(FMQ) = -0.4261*(Log_{10}(Ce^{+4}/Ce^{+3}))^4 - 0.5482*(Log_{10}(Ce^{+4}/Ce^{+3}))^3 + 1.9662*Log_{10}(Ce^{+4}/Ce^{+3}))^2 + 4.3307Log_{10}(Ce^{+4}/Ce^{+3}) - 3.1219$$ with the adequacy indicator R2 = 0.9966.

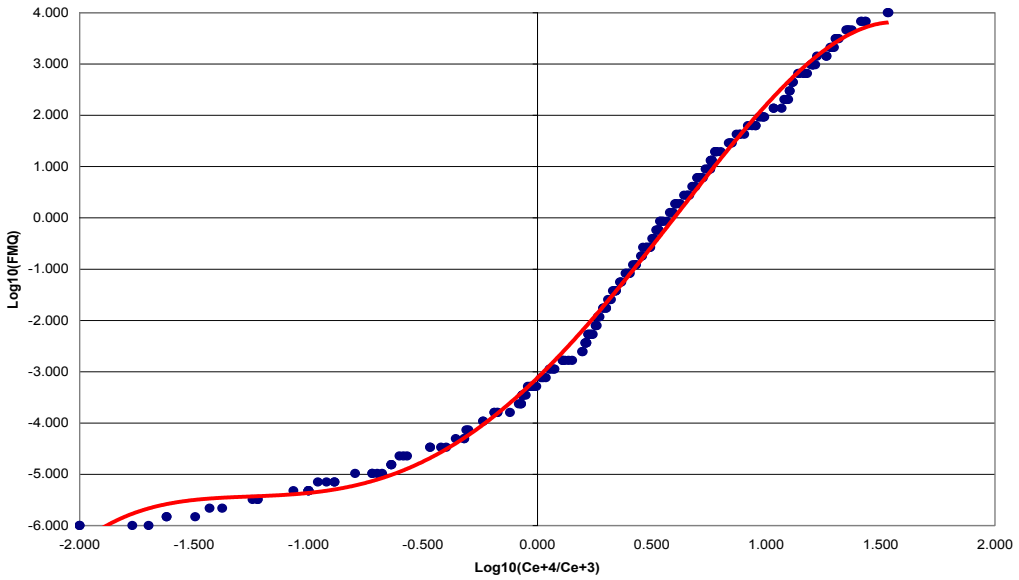

Fig. 10. Correlation between the logarithm of Ce^{+4}/Ce^{+3} to base 10 and all the calculated values (Table 2) for zircons in the FMQ buffer (blue points) and its approximation with a 4th degree polynomial (red line)

It is possible to suggest that the complex curve (Fig. 10) reflects artificial consolidation of at least two individual trends of correlation between the petrological and geochemical buffers. Using a value of -2.5 of the FMQ buffer as an average, frontier one for the division of the information into two groups, we have found two types of correlation between the two buffers (Figs. 11 and 12) that we interpreted as more reliable data for the estimation of rare-earth elements distribution in the upper and lower parts of the lithosphere. Such distribution roughly implies transsition from spinel facies of peridotite to deep garnet ones.

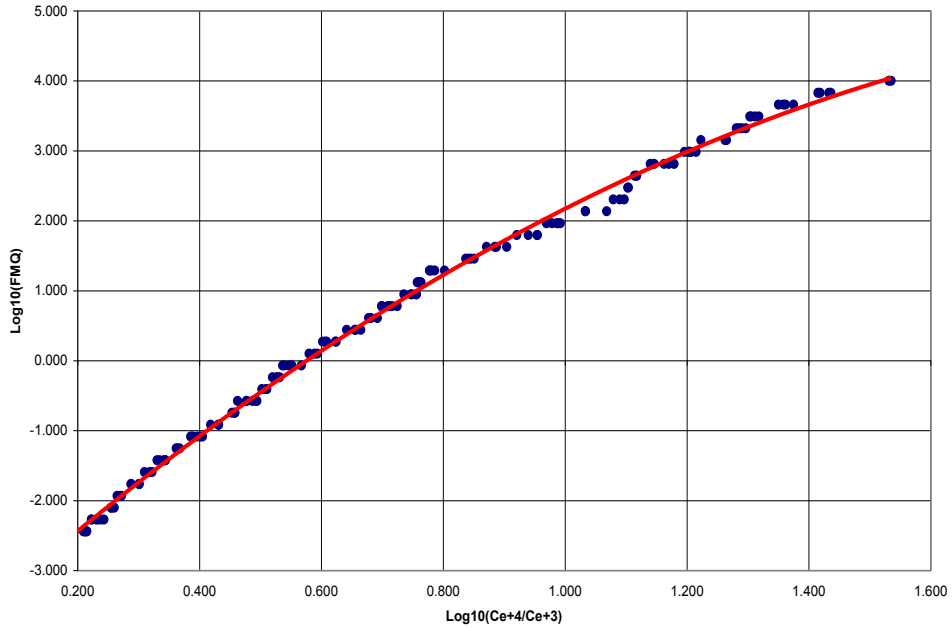

Fig. 11. Correlation between Log_{10} ($Ce^{+4}/Ce^{+3)}$ and Log_{10}(FMQ) buffer for the upper part of the lithosphere; 2^{th} degree polynom $Log_{10}(FMQ) = -1,6973 (Log_{10} (Ce^{+4}/Ce^{+3}))^2 + 7,7954 (Log_{10} (Ce^{+4}/Ce^{+3})) -3,9254$ with the adequacy indicator $R^2 = 0,9977$

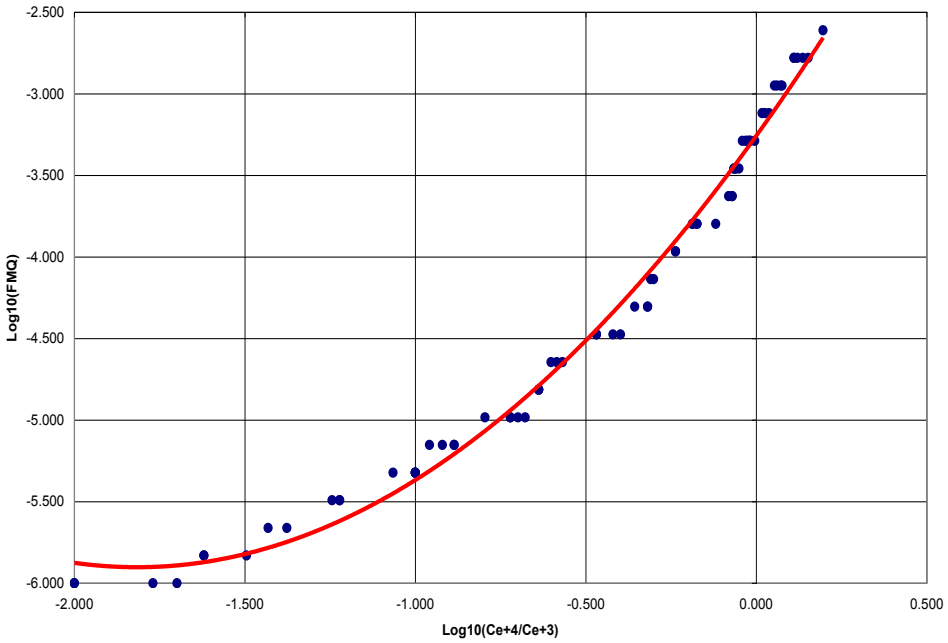

Fig. 12. Correlation between $Log_{10}(Ce^{+4}/Ce^{+3)}$ and Log_{10}(FMQ) buffer for the lower lithosphere. 2^{th} degree polynom $Log_{10}(FMQ) = 0,8014*(Log_{10}(Ce^{+4}/Ce^{+3}))^2 + 2,912*(Log_{10} (Ce^{+4}/Ce^{+3})) -3,2564$ with the adequacy indicator $R^2 = 0,9912$

This result agrees with geochronological criteria adopted for the vertical differentiation of the lithosphere. It is obvious that the given averaged data in the two buffers are simulated until validated by certain analytical findings.

8. Conclusions

Using Ce^{+4}/Ce^{+3} ratios seems to be quite promising to estimate differencies in oxygen fugacity both in the mantle and crust, as well as within the mantle the mantle section of the lithosphere since oxygen fugacity in

the two upper shells allows separating initial igneous and superimposed (secondary) generation processes for different types of rocks. It is worth emphasing that for the lower parts of the cross-section, due to the sharply reducing condition, it is typical that Ce^{+4} is almost absent, and zircons enriched with Eu^{+2} are locally present. This unique feature is clearly manifested in deep-seated kimberlitic systems. For lamproitic and basaltic zircons, this is mainly reflected in low Ce^{+4}/Ce^{+3} ratios. Nevertheless, prevalence of the reducing setting is emphasized for all the mantle rock types, and definitely points out an amplified effect of deep-seated reducing fluid flows (in the Archaean, and, possibly, in younger rocks (?)) that agrees with the petrological predictions, and is fair for the Precambrian lithosphere geochronology. It is probable that the multiple signs of secondary mantle xenoliths recrystallization cannot be confined to different P-T parameters reflecting the influence of sub-surface zones with the crust. This requires an independent discussion in near future. It is only appropriate to remind that harzburgite, lherzolite, and pyrozenite xenoliths undergone the influence of mantle metasomatism, contain increased concentrations of mobile rare elements (REE, etc.), and have higher Ce^{+4}/Ce^{+3} ratios.

This is not the only way since the geotectonic factors (subduction) sometimes add some "oxidized" substance at different levels of the lithosphere and to the deeper zones of the mantle. However, if there were conditions to inhibite such an effect, there is a possibility for a stronger estimation of mantle reducing flow parameters. The distortions of chromite xenolith FMQ buffer (Table 1) for different kimberlite pipes towards the sharper negative values (-3 to -6) predominantly relate to the measurements of the inclusions in diamonds. Such a unique level of preservation for oxygen fugacity most likely corresponds to or close to the initial reducing fluid flow from the deep-seated mantle to agree with the petrological schemes for the evolution of the lower lithosphere. It should not be neglected that formation of laying in the crust, mantle, and core of the Earth involves a series of differentiation and homogenization processes that has not been accounted for tectonic and petrological models although signs of these processes are emerging (*Balashov*, 2009a,b; *Balashov, Skublov*, 2011).

The interpretation of the oxygen fugacity contrasting nature between the upper and lower parts of the mantle lithosphere requires special attention. The zircons of the upper mantle lithosphere are believed to have formed in an oxidized setting. It is interesting that peridotites and associated rock-forming minerals demonstrate increased H_2O and OH^- concentrations with the trend preserving down to a depth of 150-160 km at FMQ varying from -1.4 to -0.1 (*Babushkina et al*., 2009). This is comparable with the Ce^{+4}/Ce^{+3} level of 2.2 to 3.9 (Table 2). Huge water reserve in the upper lithosphere being a source for water removal at increasing ocean mass through geological time, and, simultaneously, stipulates oxidation processes of the upper lithosphere rocks at increased P-T values of the lithosphere. Is this true? The issue of the crustal oxygen source in the crust and upper mantle has long been one of the most essential, but still unsolved in geochemistry and petrology of the Earth's upper shells.

One of the most important approaches to solve this issue is to correlate oxygen excess in the atmosphere resulted from a long-term period of the Earth's biosphere origin and evolution. It has recently been reflected in schemes of cyclic-polystage biosphere evolution (*Dobretsov et al*., 2006; *Sorokhtin et al*., 2010). The both schemes are conditional and demonstrate opinion of the authors on possible evolution of oxygen atmosphere, but are not confirmed by geochronological data which may describe an actual picture of oxygen fugacity. This is shown (Fig. 13) by the example of Early Precambrian granitoids and detrital zircons with Ce^{+4}/Ce^{+3} ratios close to the data for the upper mantle lithosphere (Table 2 and Fig. 11). Initial data exclude Hadean to Archaean detrital zircons in Australia (*Peck et al*., 2001): Ce^{+4}/Ce^{+3} ratios vary from 27.1 to 1.96, and Eu^{+2}/Eu^{+3} from 0.015 to 0.12 (recalculated in *Balashov, Skublov*, 2011). Similar ratios are also observed in tonalities (3813 Ma) and granodiorites (3638 Ma) from Greenland (*Whitehouse, Kamber*, 2002), i.e. for Ce^{+4}/Ce^{+3} the interval is 34 to 0.5. Thus, in the ancient crustal rocks zircons with signs of generation under high oxygen fugacity are common. It should be noted that these data, in general, reflects high heterogeneity of oxygen fugacity for the ancient crustal systems. This is also fair for zircons in younger mantle (Fig. 8 and 9) and crustal rocks, including South American subduction zones (*Ballard et al*., 2002; *Hoskin et al*., 2000, etc.). Thus, the upper mantle lithosphere and overlying crustal component represent an area of constant intensive interaction with oxygen. If oxygen was derived from the atmosphere which mass should (?) progressively grow from the Headean up to present (*Dobretsov et al*., 2006; *Sorokhtin et al*., 2010), this assumption seems to contradict actual findings (Fig. 13) for the very early Precambrian. We believe that the correlation of the evolutional stages of the biosphere with cyclic mantle and crustal magma activation of the Earth (*Balashov, Glaznev*, 2006) reflects a change in the atmospheric volatile components. This corresponds to the emergence of an abrupt sulphur excess due to the volcanogenic activation at the peak of the evolution that fatally influenced the state of the biosphere. Volcanogenic epochs are however relatively short-term, and this does not contradict oxygen synthesis by the biosphere between them. This should ultimately result in significant oxygen heterogeneity in various rock types. Existence of a wide range of Ce^{+4}/Ce^{+3} in all the surface systems of the Earth and upper mantle lithosphere is related to constant existence of exactly this heterogeneity. Alongside, various types of geological processes in the crust and mantle should have influence, or even define variation stages in the evolution of the biosphere itself. And, this has already been

noted. Another constant oxygen source along the whole interval of the Earth's history should be considered solar wind. The continuous flow of the whole range of elements, which portion in the discharge of H, C, O, and other elements to the atmosphere in a proportion close to the composition of C1 (*Anders, Grevesse*, 1989), may be regarded as quite a competitive option with other sources of oxygen at the Earth's surface especially as for the Earth's condensation and accretion stages, the flow of the solar wind is supposed to be one-two order more intensive than today (*Canuto et al*., 1983).

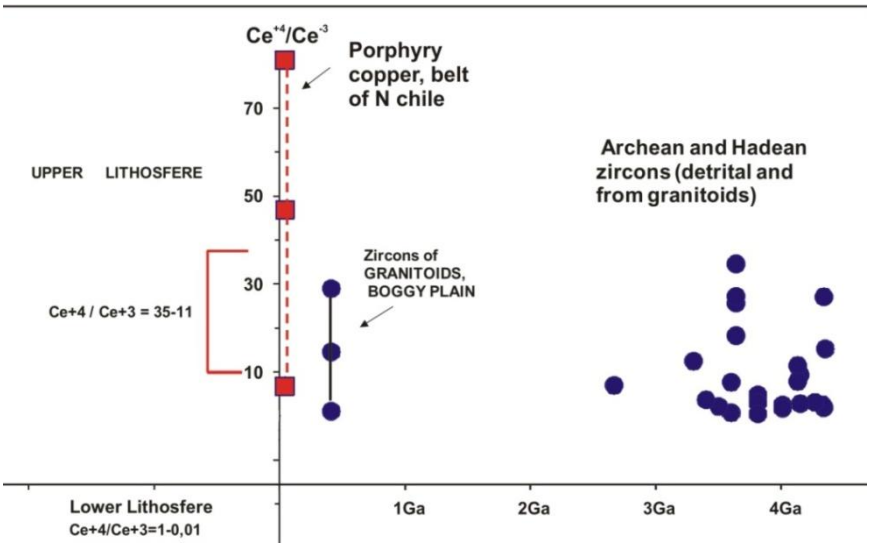

Fig. 13. Ce^{+4}/Ce^{+3} variations in zircons from the crustal rocks of various ages as compared to the zircons of the upper mantle lithosphere

The authors are grateful to I.V. Ashchepkov (PhD in Geology & Mineralogy) for certain viable remarks and suggestions, and general support of the research and Dr. E.A. Belousova for the materials on zircons from PhD Thesis, Macguarie University, Australia.

References

Anders E., Grevesse N. Abundances of the elements: Meteoritic and solar. *Geockimica et Cosmochimica Acta*, v.53, p.197-214, 1989.

Ashchepkov I.V., Vladykin N.V., Pokhilenko N.P., Logvinova A.M., Kuligin S.S., Pokhilenko I.N., Malygina L.P., Alymova N.V., Mityukhin S.I., Kopylova M. Application of the monomineral thermobarometers for the reconstruction of the mantle lithosphere structure. *In: Deep seated magmatism, its sources and plumes. Ed. by Dr. N.V. Vladykin. Miass-Irkutsk*, p.99-117, 2009a.

Ashchepkov I.V., Rotman A.Y., Nossyko S., Somov S.V., Shimupi J., Vladykin N.V., Palessky S.V., Saprykin A.I., Khmelnikova O.S. Composition and thermal structure of mantle beneath the Western Part of Congo-Kasai craton according to xenocrysts from Angola kimberlites. *Ibid.*, p.159-181, 2009b.

Ashchepkov I.V., Pokhilenko N.P., Vladykin N.V., Logvinova A.M., Rotman A.Y., Afanasiev V.P., Pokhilenko L.N., Kuligin S.S., Malygina L.V., Alymova N.V., Stegnitsky Y.B., Khmelnikova O.S. Plum interaction and evolution of continental mantle lithosphere. *Deep-seated magmatism, its sources and plumes: Proceedings of VIII International Workshop. Vladivostok-Irkutsk*, p.104-121, 2008.

Ashchepkov I.V., Vladykin N.V., Rotman A.Y., Logvinova A.M., Afanasiev V.P., Palessky V.S., Saprykin A.I., Anoshin G.N., Kuchkin A., Khmel'nikova O.S. Mir and International'naya kimberlite pipes: Trace element geochemistry and thermobarometry of mantle minerals. *Deep-seated magmatism, its sources and plumes. Ulan-Ude*, p.194-208, 2004.

Babushkina M.C., Nikitina L.P., Goncharov A.G., Ponomareva N.I. Water in mineral structures of mantle perdotites: Connection with thermal and redox conditions of the upper mantle. *Zapiski RMO*, N 1, p.3-19, 2009.

Balashov Yu.A., Martynov E.V., Balashova E.V. Ce^{+4}/Ce^{+3} variations in magmatic and secondary zircons from alkaline rocks as a sign of differences in the oxygen fugacity. *Intern. Conf. Moscow-Koktebel, Russia-Ukraine*, September 9-16, p.24-26, 2010.

Balashov Yu.A. Evolutional aspects of geochemical heterogeneity of the lithosphere. *In: Deep seated magmatism, its sources and plumes. Ed. by Dr. N.V. Vladykin. Miass-Irkutsk*, p.87-98, 2009a.

Balashov Yu.A. Vertical geochemical inhomogeneity of the lithosphere. *Complex geological and geophysical models of ancient shields. Proceedings of the All-Russian Scientific Conference. Apatity*, p.58-64, 2009b.

Balashov Yu.A., Skublov S.G. Unique indicative possibilities of cerium in zircons of different genesis. *Physical and chemical factors of petrological and ore genesis: New frontiers. Proceedings of the Conference devoted to the 110-th anniversary of the Academician RAS D.S. Korzhinsky. IGEM RAS, Moscow*, 7-9 October, p.67-70, 2009.

Balashov Yu.A., Skublov S.G. Contrasting geochemistry of igneous and secondary zircons. *Geochemistry*, N 6, p.1-12, 2011.

Balashov Yu.A., Glaznev V.N. Endogenic cycles in the crustforming problem. *Geochimia*, N 2, p.131-140, 2006.

Ballard J.R., Palin J.M., Campball I.H. Relative oxidation state of magmas inferred from Ce(IV)/Ce(III) in zircon: Application to porphyry cooper deposits of northern Chile. *Contrib. Mineral. Petrol*., v.144, p.347-364, 2002.

Ballhaus C. Redox states of lithospheric and asthenospheric upper mantle. *Contrib. Mineral. Petrol*., v.114, p.331-348, 1993.

Belousova E.A. Trace elements in zircon and apatite: Application to petrogenesis and mineral exploration. *PhD Thesis, Macquarie University, Australia*, 2000.

Belousova E.A., Griffin W.L., O'Reilly S.Y., Fisher N.I. Igneous zircon: Trace element composition as an indicator of source rock type. *Contrib. Mineral. Petrol*., v.143, p.602-622, 2002.

Belousova E.A., Griffin W.L., Pearson N.J. Trace element composition and cathodoluminescence properties of southern African kimberlitic zircons. *Mineralogical Magazine*, v.62, N 3, p.355-366, 1998.

Bogatikov O.A., Kononova V.A., Nosova A.A., Kondrashov I.A. Kimberlites and lamproites of the East European Platform: Petrology and Geochemistry. *Petrology*, v.15, N 4, p.339-360, 2007.

Burgess R., Turner G., Harris J.W. ^{40}Ar-^{39}Ar laser probe studies of clinopyroxene inclusions in eclogitic diamonds. *Geochim. Cosmochim. Acta*, v.56, p.389-402, 1992.

Canuto V.M., Levine J.S., Augustsson T.R., Imhoff C.L., Giampapa M.S. The young Sun and the atmosphere and photochemistry of the early Earth. *Nature*, v.305, p.281-286, 1983.

Dobretsov N.L., Kolchanov N.A., Suslov V.V. On the earlier stages of geosphere and biosphere evolution. *Preprint. Novosibirsk*, p.3-29, 2006.

Galimov E.M. Redox evolution of the Earth caused by a multi-stage formaton of its core. *Earth Planet. Sci. Lett.*, v.233, p.263-276, 2005.

Galimov E.M. The extension of the Earth's core as a source of internal power and an evolutional factor of redox mantle state. *Geochemistry*, N 8, p.755-758, 1998.

Glebovitsky V.A., Nikitina L.P., Vrevsky A.B. The nature of chemical inhomogeneity of the continental lithospheric mantle. *Geochemistry*, N 9, p.910-936, 2009.

Griffin W.L., Ryan C.G., Kaminky F.V., O'Reilly S.Y., Natapov L.M., Win T.T., Kinny P.D., Ilupin I.P. The Siberian lithosphere traverse: Mantle terranes and the assembly of the Siberian Craton. *Tectonophysics*, v.310, p.1-35, 1999.

Griffin W.L., O'Reilly S.Y., Abe N., Aulbach N., Davies R.M., Pearson N.J., Doyle B.J., Kili K. The origin and evolution of Archean lithospheric mantle. *Precambrian Res*., v.127, p.19-41, 2003.

Griffin W.L., Belousova E.A., Shee S.R., Pearson N.J., O'Reilly S.Y. Archean crustal evolution in the northern Yilgarn Craton: U-Pb and Hf-isotope evidence from detrital zircons. *Precambrian Res*., v.131, p.231-282, 2004.

Hoskin P.W.O., Kinny P.D., Wyborn D., Chappell B.W. Identifying accessory mineral saturation during differentiation in granitoid magmas: An integrated approach. *J. Petrology*, v.41, N 9, p.1365-1396, 2000.

Kadik A.A., Zharkova E.V., Bibikova E.V., Troneva M.A. Electrochemical measurements of inherent oxygen fugacity in the zircon crystals of different age. *Geochemistry*, N 8, p.854-860, 1998.

Kadik A.A., Litvin Yu.A., Koltashev V.V., Kryukova E.B., Plotnichenko V.G. Solubility of hydrogen and carbon in the reduced magmas of the Earth's early mantle. *Geochemistry*, N 1, p.38-53, 2006.

Kadik A.A. Regime of oxygen fugacity in the upper mantle as a reflection of chemical planetary substance differentiation. *Geochemistry*, N 1, p.63-79, 2006.

Khodorevskaya L.I. Fluid regime and behaviour of rare ore and rare-earth elements in the course of the Belomorian Fm metagabbro-norite granitization (Gorely Island, Kandalaksha Bay). *Petrology*, v.17, N 4, p.397-414, 2009.

McCammon C.A., Griffin W.I., Shee S.R. Oxidation during metasomatism in ultramafic xenoliths from the Wesselton kimberlite, South Africa: Implications for the survival of diamond. *Contrib. Mineral. Petrol*., v.141, p.287-296, 2001.

McDonough W.F., Sun S.-s. The composition of the Earth. *Chem. Geology*, v.120, p.223-253, 1995.

Pearson D.G., Shirey S.B., Bulanoa G.P., Carlson R.W., Milleodge H.J. Re-Os isotope measurements of single sulfide inclusions in a Siberian diamond and its nitrogen aggregation systematics. *Geochim. Cosmochim. Acta*, v.63, N 5, p.703-711, 1999.

Peck W.H., Valley J.W., Wilde S.A., Graham C.M. Oxygen isotope ratios and rare earth elements in 3,3 to 4,4 Ga zircons: Ion microprobe evidence for high $\delta^{18}O$ continental crust and oceans in the Early Archean. *Geochim. Cosmochim. Acta*, v.65, N 22, p.4215-4229, 2001.

Rodionov D.A. Statistical methods of geological object differentiation in accordance with a set of evidences. *M., Nedra*, p.36-48, 1968.

Rubanova E.V., Griffin W.L., O'Reilly S.Y. Origin of diamondites. *Geochemistry of magmatic rocks. XXVII International Conf. School "Geochem. of Alkaline rocks". Abstr., Moscow-Koktebel, Russia-Ukraina*, September 9-16, p.149-150, 2010.

Ryabchikov I.D. Regime of volatile components in the zones of diamond formation. *In: Deep seated magmatism, its sources and plumes. Ed. by Dr. N.V. Vladykin*. *Miass-Irkutsk*, p.80-86, 2009.

Ryabchikov I.D., Kogarko L.N. The redox potential of the Khibiny igneous system and genesis of abiogenous hydrocarbons in the alkaline plutons. *Geology of ore deposits*, v.51, N 6, p.475-491, 2009.

Ryabchikov I.D., Kogarko L.N., Solovova I.P. Physical and chemical settings of magma formation at the base of the Siberian plume in accordance with the research data for microinclusions in meimechite and alkaline picrites of the Maimecha+Kotuy province. *Petrology*, v.17, N 3, p.311-323, 2009.

Skublov S.G., Lobach-Zhuchenko S.B., Guseva N.S., Gembitskaya I.M., Tolmachyova E.V. Distribution of rare-earth and rare elements in zircons from the miaskite lamproites of the Panozero intrusion in Central Karelia. *Geochemistry*, N 9, p.958-971, 2009.

Sobolev A.V., Krivolutskaya D.V., Kuzmin D.V. Petrology of parental melts and mantle magma sources in the Siberian trappean province. *Petrology*, v.17, N 3, p.276-310, 2009.

Sorokhtin O.G., Chilingar G.V., Sorokhtin N.O. Theory of development of the Earth… *Moscow-Izhevsk, Scientific Center, Regular and chaotic dynamics, Institute of computer studies*, 751 p., 2010.

Smith C.B. Pb, Sr and Nd isotopic evidence for sources of southern African Cretaceous kimberlites. *Nature*, v.304, p.51-54, 1983.

Takahashi Y., Shimizu H., Kagi H., Yoshida H., Usui A., Nomura M. A new method for the determination of Ce^{III}/Ce^{IV} ratios in geological materials: Application for weathering, sedimentary and diagenetic processes. *Earth Planet. Sci. Lett*., v.182, p.201-207, 2000.

Zheng J., Griffin W.L., O'Reily S.Y., Zhang M., Pearson N. Zircons in mantle xenoliths the Triassic Yangtze-North China continental collision. *Earth Planet. Sci. Lett*., v.247, p.130-142, 2006.

Yatsenko G.M., Panov B.S., Belousova E.A., Lesnov F.P., Griffin U.L., Slivko E.M., Rosikhina A.I. Distribution of rare-earth elements in zircons from minettes of the Kirovograd Block (Ukraine). *DAN*, v.370, N 4, p.524-528, 2000.

Whitehouse M.J., Kamber B.S. On the overabundance of light rare earth elements in terrestrial zircons and its Earth's earliest magmatic differentiation. *Earth Planet. Sci. Letters*, v.204, p.333-346, 2002.